

Endogenous cannabinoids mediate retrograde signalling at hippocampal synapses

Rachel I. Wilson & Roger A. Nicoll

Departments of Cellular and Molecular Pharmacology and Physiology, University of California, San Francisco, California 94143, USA

Marijuana affects brain function primarily by activating the G-protein-coupled cannabinoid receptor-1 (CB1)¹⁻³, which is expressed throughout the brain at high levels⁴. Two endogenous lipids, anandamide and 2-arachidonylglycerol (2-AG), have been identified as CB1 ligands^{5,6}. Depolarized hippocampal neurons rapidly release both anandamide and 2-AG in a Ca²⁺-dependent manner⁶⁻⁸. In the hippocampus, CB1 is expressed mainly by GABA (γ -aminobutyric acid)-mediated inhibitory interneurons, where CB1 clusters on the axon terminal⁹⁻¹¹. A synthetic CB1 agonist depresses GABA release from hippocampal slices^{10,12}. These findings indicate that the function of endogenous cannabinoids released by depolarized hippocampal neurons might be to downregulate GABA release. Here we show that the transient suppression of GABA-mediated transmission that follows depolarization of hippocampal pyramidal neurons¹³ is mediated by retrograde signalling through release of endogenous cannabinoids. Signalling by the endocannabinoid system thus represents a mechanism by which neurons can communicate backwards across synapses to modulate their inputs.

Three properties of 'depolarization-induced suppression of inhibition' (DSI)¹³ suggested a role for cannabinoids in DSI. First, DSI, like endocannabinoid synthesis, requires Ca²⁺ influx into the postsynaptic neuron¹⁴. Second, DSI expression is probably presynaptic, as DSI does not affect the sensitivity of the postsynaptic membrane to iontophoresed GABA, or the quantal size of miniature GABA-mediated events^{13,15,16}, consistent with the localization of CB1 to GABA-containing axon terminals. Last, DSI is blocked by pertussis toxin¹⁷, implying a function for a G_i- or G_o-coupled receptor such as CB1. We therefore asked whether CB1 antagonists block DSI. We recorded from single CA1 pyramidal neurons in hippocampal slices in the whole-cell configuration. Figure 1a shows the transient depression of evoked inhibitory postsynaptic currents (eIPSCs) caused by a brief depolarizing step in the holding potential of a CA1 pyramidal neuron; incubating slices in the CB1 antagonist AM251 (Tocris) abolishes this effect. Figure 1b summarizes the effects of AM251 and another CB1 antagonist, SR141716 (National Institute on Drug Abuse), on DSI magnitude. SR141716 also blocked DSI induced by a train of action potentials (1 s, 20 Hz) rather than a voltage step (data not shown). Acute applications of SR141716 blocked the ability of a depolarizing step to depress eIPSC amplitude without affecting baseline eIPSCs (Fig. 1d). Furthermore, the effect of DSI on inhibitory transmission was mimicked by a synthetic CB1 agonist, WIN55212-2 (RBI), which acutely depressed baseline eIPSC amplitude (Fig. 1e). Pre-incubation in AM251 blocked this depression (eIPSC amplitude 95 ± 3% of baseline after 20 min of WIN55212-2 exposure (*n* = 6); data not shown, *P* < 0.05, compared with slices without AM251, paired *t*-test). WIN55212-2 did not affect the DSI-resistant component of the eIPSC (Fig. 1e), and thus occluded DSI.

The natural CB1 ligand 2-AG (Biomol) had only a small effect compared with the synthetic agonist (Fig. 2a), suggesting that 2-AG was not reaching sufficient concentrations in the slice. This is consistent with a recent report that both 2-AG and anandamide are substrates for an endogenous transporter that removes these ligands from the extracellular space^{18,19}. Application of AM404

(Tocris), an inhibitor of the anandamide/2-AG transporter, depressed baseline eIPSC amplitude without affecting the DSI-resistant component of the eIPSC (Fig. 2b). Pre-incubation of slices in SR141716 abolished the effects of AM404 (Fig. 2c). As AM404 is not itself a CB1 agonist¹⁸, these results imply that the endogenous substrate for the AM404-sensitive transporter is a cannabinoid that mimics and occludes DSI when allowed to accumulate in the slice. As a CB1 antagonist has no effect on baseline eIPSCs (Fig. 1d), tonic synthesis of endogenous cannabinoids must be normally balanced by uptake, which keeps extracellular cannabinoid levels below that required for CB1 activation. The kinetics of DSI were not changed as AM404 washed into the slice (Fig. 2d), suggesting that the AM404-sensitive transporter does not clear the retrograde signal rapidly enough to affect DSI decay. The kinetics of DSI probably reflect signal-transduction events inside the presynaptic terminal, or else passive diffusion of cannabinoids away from the site of release.

If an endogenous cannabinoid mediates DSI, then a CB1 agonist and DSI must depress GABA-mediated transmission by the same mechanism. We therefore asked whether DSI and WIN55212-2 act at a similar locus. In those experiments where WIN55212-2 depressed eIPSCs by at least 40%, the amplitude ratio of two closely

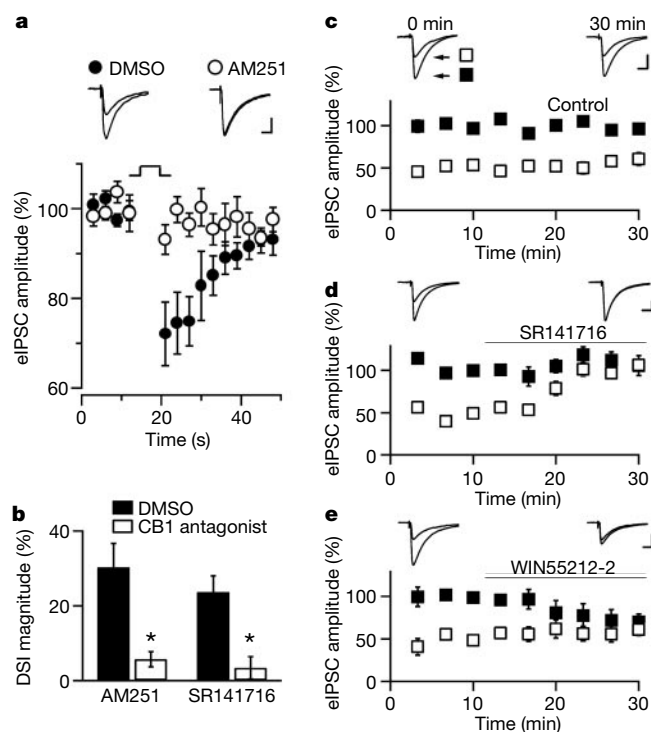


Figure 1 DSI requires endogenous cannabinoids. **a**, In pyramidal neurons (*n* = 14) from slices pre-incubated in AM251 (2 μM), a 5-s depolarizing step results in little or no suppression of eIPSCs. Interleaved DMSO controls (*n* = 17) show a robust suppression. Average of 5 trials per cell. Insets show average IPSCs for the 10 s before and 10 s after the depolarizing step. **b**, Effect of AM251 (6 ± 2% versus 30 ± 6% average DSI in AM251 and DMSO alone, respectively) and SR141716 on DSI (2 μM: 3 ± 3% versus 24 ± 4% average DSI in SR141716 (*n* = 11) and DMSO (*n* = 10) alone, respectively). Asterisk, *P* < 0.005. **c-e**, Control experiments (*n* = 7) (**c**) show stable DSI over 30 min, whereas SR141716 (*n* = 6) (**d**) blocks DSI by antagonism, and WIN55212-2 (800 nM: *n* = 5) (**e**) blocks DSI by occlusion (average DSI magnitude at 30 min in controls is 70 ± 10% of magnitude during baseline, compared with 11 ± 10% in SR141716 slices, and 19 ± 9% in WIN55212-2 slices; *P* < 0.005 for both treatments). Scale bars: **a, c-e**, 200 pA, 20 ms. The statistical test used was the paired *t*-test. Filled squares, eIPSC amplitude just before 5-s depolarization; open squares, eIPSC amplitude just after 5-s depolarization.

spaced eIPSCs (the paired-pulse ratio, PPR) was significantly increased (Fig. 3a). Similarly, DSI also reversibly increased PPR (Fig. 3b), which generally correlates with a local decrease in the probability of vesicular release from the axon terminal. In agreement with a previous study¹², we also found that WIN55212-2 decreases the frequency of Ca²⁺-dependent miniature IPSCs (mIPSCs) recorded after blockade of action potentials by tetrodotoxin (TTX), and in the presence of high external potassium and Ca²⁺ concentrations (Fig. 3c, d). In the same conditions, but without TTX, depolarizing the postsynaptic cell induces a significant decrease in action-potential-driven spontaneous IPSCs (sIPSCs) (Fig. 3e). After adding TTX to the bath, depolarization elicits a similar depression of mIPSC frequency (Fig. 3e, f). Consistent with a presynaptic locus, DSI does not affect mIPSC amplitude (100 ± 3% of baseline (*n* = 5); data not shown). Thus DSI, like the CB1 agonist, seems to act locally at the presynaptic terminal.

The conclusion that DSI is mediated by endogenous cannabinoids leads to three predictions about the properties of DSI. First, as both anandamide and 2-AG exit the cell by diffusion and/or passive transport, release of the retrograde signal in DSI should not require vesicular fusion⁸. We filled the postsynaptic cell by means of the recording electrode with botulinum toxin E light chain (BTE) while

monitoring DSI. BTE proteolytically cleaves both the synaptosome-associated proteins SNAP-25 and SNAP-23 (refs 20, 21); either of these is a necessary component of the minimal machinery required for all cellular membrane fusion²². We found that BTE does not affect the stability of DSI (Fig. 4a). As a control, we incubated recombinant SNAP-25 with BTE in our electrode-filling solution; the concentration of BTE used in our recordings was in ten-fold excess over that required to cleave all the SNAP-25 within 1 h (Fig. 4b). DSI is also unaffected by botulinum toxin B light chain (BTB) (Fig. 4a), which cleaves the vesicle-associated membrane protein VAMP2 and disrupts vesicular fusion in pyramidal cell dendrites when added to the solution in the recording electrode^{23,24}.

As the trigger for cannabinoid synthesis is cytoplasmic Ca²⁺, a second prediction is that Ca²⁺ alone should be sufficient to trigger

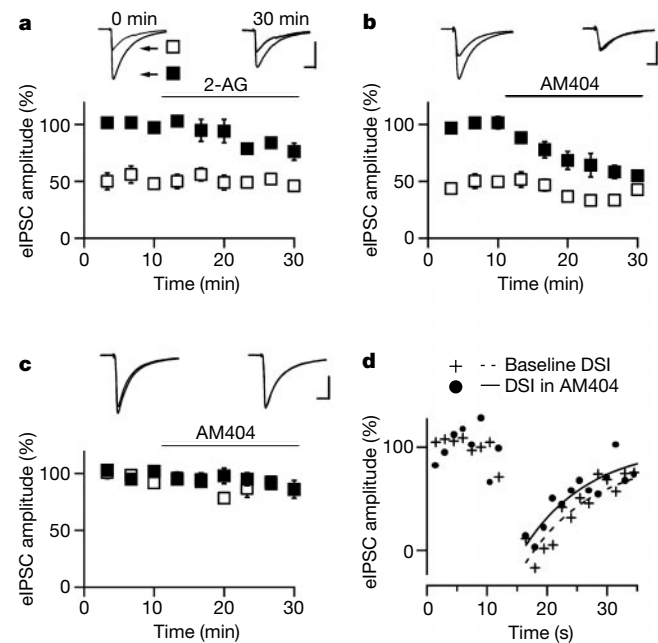


Figure 2 DSI is mimicked and occluded by blocking uptake of endogenous CB1 ligands. **a**, Effect of 2-AG on eIPSCs (30 μM: 76 ± 7% of baseline at 30 min, (*n* = 6) *P* < 0.05, compared with controls in Fig. 1c). **b**, AM404 significantly depresses eIPSCs (20 μM: 55 ± 5% of baseline at 30 min, (*n* = 6) *P* < 0.001, compared with controls in Fig. 1c) and partially occludes DSI (average DSI magnitude at 30 min is 39 ± 11% of magnitude during baseline, *P* < 0.05, compared with DSI from controls in Fig. 1c). **c**, Depression of eIPSCs by AM404 is antagonized by pre-incubation with SR141716 (eIPSC amplitude 85 ± 4% of baseline at 30 min, (*n* = 5) *P* < 0.005, compared to slices without SR141716). **d**, AM404 does not significantly affect the kinetics of DSI. Average time course of DSI during baseline period compared to the first 12 min of AM404 wash-in, during which DSI is being progressively occluded, is shown (*n* = 6, average of 4–5 baseline trials and 6 AM404 trials per cell). Lines are single exponential fits to the data (dashed line: baseline DSI, τ = 22.5 s; solid line: DSI during first 12 min of AM404 wash-in, τ = 21.8 s; not significantly different by a within-cell comparison of τ , *P* > 0.7, paired *t*-test). Scale bars: **a–c**: 200 pA, 20 ms. DSI = DSI_{max}e^{-t/τ}.

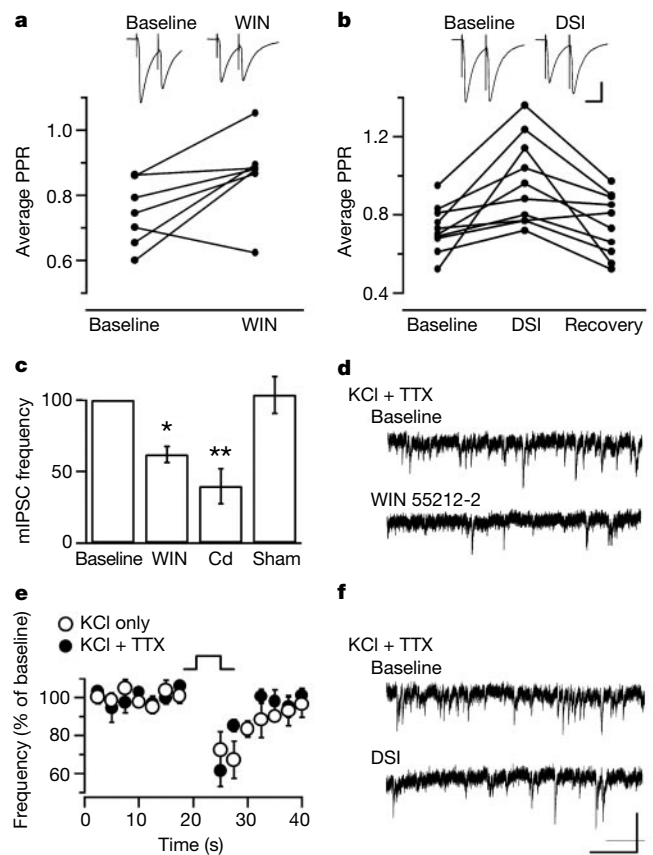


Figure 3 DSI and a CB1 agonist suppress IPSCs by the same mechanism. **a**, In experiments where WIN55212-2 depressed eIPSCs by at least 40%, the paired-pulse ratio (PPR) was significantly increased (inter-pulse interval 55 ms; (*n* = 7) *P* < 0.05). **b**, DSI reversibly increases the PPR of eIPSCs (inter-pulse interval 55 ms; (*n* = 10) *P* < 0.01). Scale bar: 200 pA, 40 ms. **c**, **d**, WIN55212-2 decreases the frequency of mIPSCs recorded in TTX, high external calcium, and high external potassium (62 ± 6% of baseline frequency 20 min after wash-on; *n* = 6). CdCl₂ (Cd) further decreases mIPSC frequency under these conditions (40 ± 12% of baseline frequency compared with either baseline or WIN55212-2; *n* = 5) Asterisk, *P* < 0.005; double asterisk, *P* < 0.05. No change in mIPSC frequency occurred over 20 min when no drug was applied (Sham) (104 ± 13% of baseline; *n* = 4). **e**, **f**, Under the same conditions of elevated calcium and potassium, but without TTX, depolarizing a pyramidal cell depresses action-potential-dependent sIPSCs (sIPSC frequency 74 ± 7% of baseline, *P* < 0.001; sIPSC amplitude 87 ± 6% of baseline, (*n* = 5) *P* < 0.05; data not shown). After adding TTX, depolarizing the same cell causes a similar decrease in mIPSC frequency (77 ± 4% of baseline; (*n* = 5) *P* < 0.005). Scale bar: 50 pA, 1 s. The statistical test used was the paired *t*-test.

DSI. We find that the effect of a depolarizing step (Fig. 4c) is indistinguishable from the effect of uncaging Ca^{2+} from a photolabile chelator when the pyramidal neuron is not depolarized (Fig. 4d). Like DSI¹³, Ca^{2+} uncaging transiently depresses both the frequency and amplitude of sIPSCs (Fig. 4e). Ca^{2+} uncaging also depresses eIPSCs, an effect that is antagonized by AM251 (Fig. 4f). Like DSI, Ca^{2+} -induced depression is expressed presynaptically, as the amplitude of mIPSCs elicited by sucrose (150 mM) in the presence of TTX (1 μ M) is unaffected ($97 \pm 4\%$ of baseline, measured 6 s after flash ($n = 8$); data not shown).

On the basis of reports that DSI is attenuated by the metabotropic glutamate receptor (mGluR) antagonist (S)- α -methyl-4-carboxyphenylglycine((S)-MCPG)²⁵, it has been suggested that the retro-

grade signal in DSI might be glutamate, although not all studies have found a role for mGluRs in DSI²⁶. Glutamate, or any other classical neurotransmitter, could be released from pyramidal cell somata by either vesicular fusion or by reversal of an electrogenic transporter on the plasma membrane. However, our data imply that neither of these processes can account for the release of the retrograde signal. We therefore re-examined the sensitivity of DSI to mGluR antagonists. The broad-spectrum, high-affinity mGluR antagonist LY341495 (Tocris) did not affect DSI (Fig. 4g). DSI was also resistant to (S)-MCPG (Tocris), although this dose significantly diminished the depression of eIPSCs by glutamate iontophoresed from a second electrode near the recorded cell (Fig. 4h). Our results are inconsistent with the hypothesis that glutamate, or indeed any classical neurotransmitter, is the primary retrograde signal in DSI. Although mGluRs seem not to be required for DSI, our results do not rule out the possibility that mGluRs might have a modulatory function in DSI. Indeed, recent data suggests that mGluR activation can enhance DSI in hippocampal slices (B. E. Alger, personal communication). Differences in experimental preparations could produce different levels of mGluR activation, and could explain the variability in the effect of

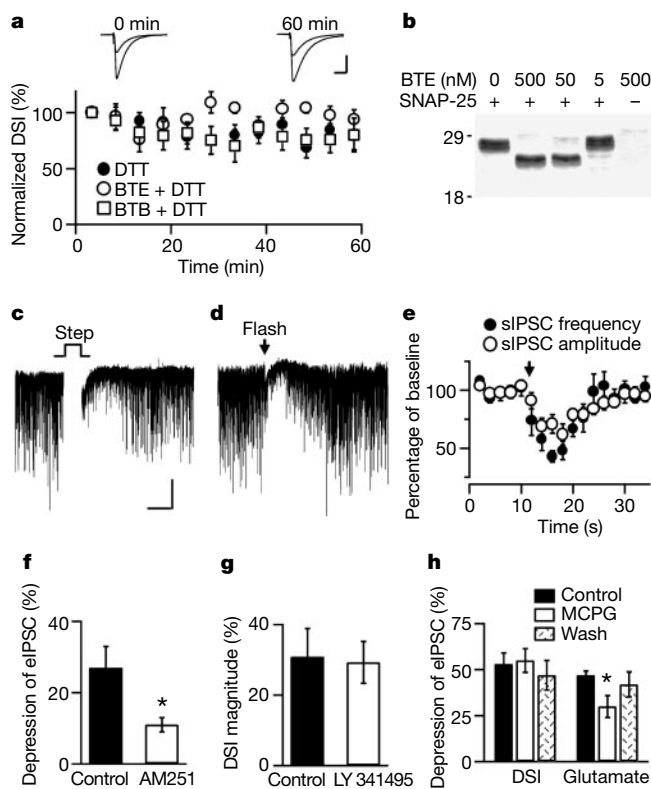


Figure 4 The postsynaptic properties of DSI are consistent with cannabinoids but inconsistent with a classical neurotransmitter. **a**, Filling pyramidal neurons with BTE ($n = 5$) or BTB ($n = 7$) (500 nM), plus DTT to maximize botulinum toxin activity, had no effect on the stability of DSI compared to DTT ($n = 8$) alone (DSI magnitude at 60 min was $94 \pm 9\%$ of the average magnitude during first 5 min for BTE and $80 \pm 15\%$ for BTB; versus $81 \pm 14\%$ for control). Scale bar: 200 pA, 20 ms. The mean absolute magnitudes of DSI were $52 \pm 3\%$ (BTE), $45 \pm 3\%$ (BTB) and $59 \pm 7\%$ (control). **b**, 50 nM BTE was sufficient to completely cleave in 60 min all the SNAP-25 diluted in a sample of electrode-filling solution. Relative molecular mass (K) shown on left. **c, d**, Depolarizing a pyramidal neuron (**c**) and photolysing caged calcium inside a pyramidal neuron (**d**) had similar effects on sIPSCs. Scale bar: 50 pA, 10 s. **e**, Both sIPSC frequency and sIPSC amplitude were transiently depressed by calcium uncaging (frequency $43 \pm 5\%$ of baseline, amplitude $71 \pm 8\%$ of baseline, both measured 6 s after flash; $n = 8$ cells). **f**, AM251 (2 μ M) antagonizes the depression of eIPSCs elicited by calcium uncaging ($11 \pm 2\%$ average depression in AM251 ($n = 15$), versus $27 \pm 6\%$ average depression in DMSO alone, ($n = 16$)). Asterisk, $P < 0.01$, *t*-test. **g**, DSI is normal in slices pre-incubated and recorded in LY341495 (50 μ M) ($29 \pm 6\%$ average DSI; $n = 10$) compared to controls ($31 \pm 8\%$ average DSI; $n = 10$). **h**, (S)-MCPG (5 mM) does not affect DSI ($53 \pm 6\%$ average DSI during baseline versus $55 \pm 6\%$ in (S)-MCPG; $n = 6$), although it reduces the depression of eIPSCs by iontophoresed glutamate in the same recordings ($47 \pm 2\%$ average depression during baseline versus $30 \pm 6\%$ in (S)-MCPG). Asterisk, $P < 0.05$, paired *t*-test.

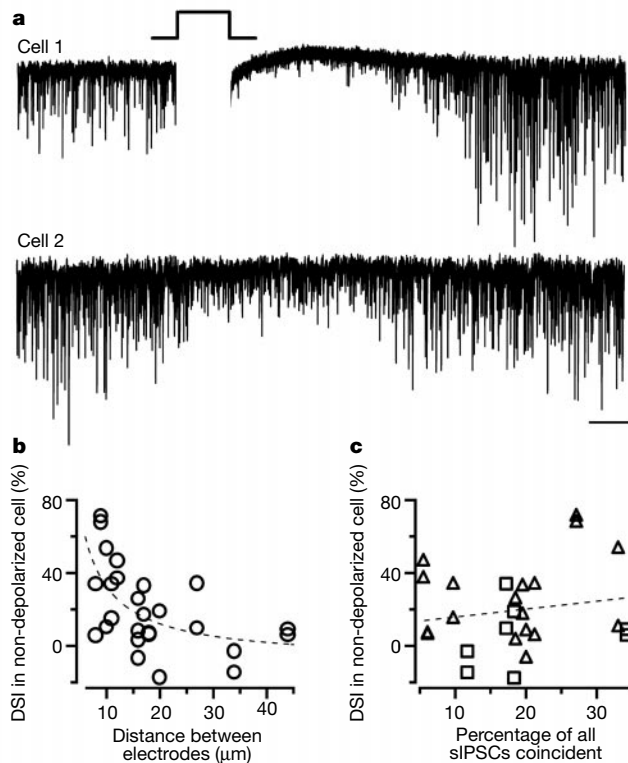


Figure 5 The retrograde signal in DSI can disinhibit nearby neurons. **a**, Depolarizing one CA1 pyramidal neuron for 5 s results in a transient suppression of sIPSCs (cell 1). The trace is blanked during the depolarizing step for clarity. A pyramidal cell 9 μ m away (cell 2) also showed suppression of sIPSCs, beginning about 1 s after cell 1 was depolarized. Scale bar: 100 pA, 5 s. **b**, In 13 pyramidal cell pairs, the suppression of sIPSCs in the non-depolarized cell was steeply related to its distance from the depolarized cell, with little propagation beyond 20 μ m ($r^2 = 0.34$, DSI in non-depolarized cell versus 1/distance; $P < 0.005$, analysis of variance). The dotted line is a linear fit of DSI in the non-depolarized cell versus 1/distance. **c**, In the same pairs, suppression of sIPSCs in the non-depolarized cell was not related to the degree of shared presynaptic input, assessed by the percentage of sIPSCs in both cells during the baseline period, which had a coincident event in the other cell ($r^2 = 0.03$, DSI in non-depolarized cell versus percentage sIPSCs coincident; not significant, analysis of variance). The dotted line is a linear fit of DSI in the non-depolarized cell versus percentage coincidence. Triangles, close pairs ($< 20 \mu$ m apart); squares, more distant pairs.

mGluR antagonists.

Endogenous cannabinoids are small diffusible molecules. A third prediction, therefore, is that DSI ought to spread. To test this, we recorded simultaneously in whole-cell mode from pairs of nearby pyramidal neurons. When depolarizing one of these two neurons depressed sIPSCs in that cell, a simultaneous depression of sIPSCs was often observed in the non-depolarized neighbour (Fig. 5a). We made 13 pairs of simultaneous recordings (26 neurons) where both neurons in the paired recording could produce DSI of their own IPSCs, signifying that these neurons were able to produce the retrograde signal and had presynaptic inputs sensitive to the signal. Of these 26 neurons, 10 showed an average suppression of inhibition of at least 20% immediately after the other neuron in the pair was depolarized. The degree of DSI propagation in these pairs is dependent on distance, with 9 of the 10 propagating pairs separated by 20 μm or less (Fig. 5b).

A DSI-like phenomenon in cerebellar Purkinje cells²⁷ and cultured myocytes²⁸ involves retrograde messengers that locally initiate a signalling cascade in the presynaptic axon terminal; this then propagates the depression through that axon to other synapses. If hippocampal DSI shared this property, then propagation should depend on the degree to which the two postsynaptic cells share some presynaptic inputs, as estimated by the percentage of sIPSCs in the two cells that are coincident. We find that the degree of propagation is uncorrelated with this variable (Fig. 5c), consistent with propagation occurring mainly through a diffusible molecule capable of spreading through a sphere of about 40 μm in diameter. This profile is consistent with the properties of the endocannabinoids, whose sphere of diffusion is limited by uptake, and hindered by their lipophilicity⁸.

Here we have placed cannabinoids in a small group of molecules identified as fast retrograde signals in the mature nervous system. Furthermore, our study represents the first identification of a physiological process mediated by endogenous brain cannabinoids. CB1-expressing interneurons are thought to control hippocampal oscillations in the theta and gamma frequency, and a CB1 agonist decreases the power of synchronous oscillations in hippocampal slices¹¹, suggesting that endogenous cannabinoids may modulate the synchronous spiking of hippocampal cells. Moreover, as decreasing GABA-mediated inhibition promotes long-term potentiation of glutamatergic synapses²⁹, DSI may facilitate learning under conditions of intense hippocampal recruitment. The fact that only strong depolarization can induce DSI means that relevant levels of cannabinoids probably occur in response to particularly intense stimuli. By contrast, exogenous cannabinoids such as marijuana might be predicted to tonically disinhibit the hippocampus, thereby destroying the information contained in the feedback loop of DSI and promoting a noisier, more random pattern of synaptic modification.

Note added in proof: It has come to our attention that two papers showing a role for endocannabinoids are being published in *Neuron* (Kreitzer, A. C. & Regehr, W. G. *Neuron*, **29**, 717–727; 2001 and Ohno-Shosaku, T., Maejima, T. & Kano, M. *Neuron*, **29**, 729–738; 2001). □

Methods

Slice preparation and electrophysiology

Transverse hippocampal slices (300 μm) were obtained from Sprague–Dawley rats (P16–30) and maintained in artificial cerebrospinal fluid (ACSF) for at least 1 h before recording. ACSF contained (in mM): 119 NaCl, 26 NaHCO₃, 10 glucose, 3 KCl, 2.5 CaCl₂, 2 MgSO₄, 1 NaH₂PO₄, 0.005 NBQX (Tocris), 0.002 CPP (Tocris), and was equilibrated with 95% O₂ and 5% CO₂ at 20–22 °C. We added carbachol (5–10 μM ; RBI) to the ACSF in some experiments (Figs 4c–e and 5) to increase sIPSC frequency¹⁷. Recording electrodes were filled with a solution of (in mM): 100 CsCH₃SO₃, 60 CsCl, 5 QX-314 chloride, 10 HEPES, 0.2 EGTA, 1 MgCl₂, 1 Mg-ATP, and 0.3 Na₃GTP (pH 7.3, 275 mOsm). Synaptic currents were filtered at 2 kHz and collected at 5 kHz. When series resistance exceeded 40 M Ω or input resistance fell below 100 M Ω , experiments were terminated. IPSCs were elicited using bipolar tungsten electrodes in or near CA1 stratum pyramidale. DSI tests, performed every 120 s, consisted of 30 stimuli at 0.33 Hz, with depolarization from

–60 mV to 0 mV for 5 s after the eighth stimulus. DSI was calculated using the mean of the three eIPSCs just before the depolarization ($\text{amp}_{\text{baseline}}$) and the three eIPSCs just after the depolarization (amp_{test}): $\text{DSI} (\%) = 100(1 - (\text{amp}_{\text{test}}/\text{amp}_{\text{baseline}}))$.

Pharmacology

Slices were pre-incubated with the drug AM251 (Figs 1a, b and 4f), SR141716 (Fig. 1b) or LY341495 (Fig. 4g) for 45–150 min, and recordings were performed in the presence of the same concentration. Drug-treated slices were interleaved with control slices from the same animal incubated for an equivalent period of time in the same concentration of the solvent (water, dilute NaOH, or DMSO) used to make the drug stock. Overall, about 60% of cells have significant DSI, with DSI in these cells averaging about 50% in magnitude; thus, DSI averaged about 30% in control experiments. For acute applications of drugs (Figs 1c–e and 2a–d), cells were discarded immediately if they did not show DSI of at least 30% during the 10-min baseline period.

Miniature IPSCs

In experiments examining mIPSCs (Fig. 3c–f) additional KCl (2.0–7.5 mM) was added to the ACSF at the beginning of the experiment until sIPSC frequency was at least 3 Hz. The ACSF in these experiments included high Ca²⁺ (7.5 mM total Ca²⁺) and low magnesium concentration (0.1 mM total Mg²⁺) to maximize the probability of release, whereas high total divalents served to decrease action-potential initiation. This permitted us, in DSI experiments (Fig. 3e–f), to record both action-potential-dependent sIPSCs and, after addition of TTX, mIPSCs at a frequency of 3–10 Hz without changing external KCl concentrations. Phosphate was omitted from the ACSF. In DSI experiments (Fig. 3e–f), cells showing DSI of eIPSCs measuring less than 30% on the first test (before addition of high external KCl) were discarded immediately. Although the cells selected for these experiments (Fig. 3e–f) all had robust DSI in normal ACSF (initial average DSI was 60 \pm 4% before adding high potassium), elevating external potassium decreased the magnitude of DSI, such that the effect on sIPSC frequency and amplitude was modest, although highly significant. This is consistent with reports that depolarization decreases the efficacy of G-protein-mediated inhibition of voltage-dependent calcium currents³⁰, and may explain the failure of one study¹³ to find an effect of DSI on Ca²⁺-dependent mIPSCs, as even higher concentrations of external potassium were used.

A related issue is why we found an increase in the PPR during DSI, whereas other reports^{15,16} have not. In contrast to previous studies, we used a shorter inter-pulse interval (55 ms versus 200 ms) to maximize interaction between the two stimuli, and we used a paired *t*-test, which has better statistical resolution than an unpaired comparison. Finally, we note that under optimal conditions DSI might block completely transmission at the subset of terminals expressing CB1 and that, in these cases, a change in the PPR would not be expected.

Botulinum toxins and Ca²⁺ uncaging

BTE (500 nM; a gift from R. Scheller) light chain or BTB (500 nM; List Biolabs) light chain were dissolved in electrode-filling solution with 5 mM dithiothreitol (DTT). We performed recordings at 31 °C. Cells with DSI of less than 30% on the first test (1 min after break-in) were discarded immediately. For Fig. 4b, recombinant SNAP-25 (a gift from R. Scheller) was diluted to a concentration of 0.2 mg ml⁻¹ in electrode-filling solution, along with 5 mM DTT and 0–500 nM BTE. After incubation for 60 min at 31 °C, proteins were separated on a 12% polyacrylamide gel and stained with Coomassie blue. In Ca²⁺-uncaging experiments (Fig. 4c–e) recording electrodes were filled with a solution containing (in mM): 100 CsCH₃SO₃, 78 tetraethylammonium chloride, 5 QX-314 chloride, 25 HEPES, 1 MgCl₂, 2 Mg-ATP, 0.3 Na₃GTP, 5 nitrophenyl-EGTA (Molecular Probes), 4 CsOH, 2 CaCl₂. Apamin (100 nM; CalBiochem) was included in the ACSF. Internal tetraethylammonium and external apamin were used to block Ca²⁺-dependent potassium conductances after uncaging. To uncage nitrophenyl-EGTA, cells were exposed for 800 ms to ultraviolet light from a 100 W mercury burner (Olympus) passed through a 25% neutral density filter.

Paired recordings

We made 39 pairs of simultaneous recordings from CA1 pyramidal neurons (78 neurons); 44 of the 78 (56%) were able to induce DSI of their own IPSCs. This percentage is consistent with the finding that only a subpopulation of interneurons expresses CB1 (ref. 10). Of these 44 neurons, 26 were members of a pair where both neurons were able to produce DSI of their own IPSCs. We analysed this set of recordings to determine under what conditions DSI might spread. The distance between neurons was defined as the distance between the tips of the two recording electrodes. Coincident sIPSCs were defined as events whose peak amplitude occurred within 7 ms of each other. A 7-ms window was chosen because longer windows did not substantially increase the frequency of calculated coincidence, whereas shorter windows did substantially decrease that frequency; also, average sIPSC rise time sometimes differed by 2–4 ms between the two cells, probably owing to different series resistances. As DSI of sIPSCs is a decrease in both frequency and amplitude of events, we express DSI here as a function of charge transfer normalized to time, that is, the sum of the areas of all sIPSCs in a period of time divided by the number of seconds in that period. Thus, expressed as a percentage decrease: $\text{DSI}(\%) = 100(1 - (\text{charge transfer}_{\text{test}}/\text{charge transfer}_{\text{baseline}}))$ where the baseline period was the 20 s immediately preceding the depolarization, and the test period was the 15 s immediately after the depolarization.

Received 11 December 2000; accepted 6 February 2001.

- Matsuda, L. A., Lolait, S. J., Brownstein, M. J., Young, A. C. & Bonner, T. I. Structure of a cannabinoid receptor and functional expression of the cloned cDNA. *Nature* **346**, 561–564 (1990).
- Caulfield, M. P. & Brown, D. A. Cannabinoid receptor agonists inhibit Ca current in NG108-15 neuroblastoma cells via a pertussis toxin-sensitive mechanism. *Br. J. Pharmacol.* **106**, 231–232 (1992).
- Mackie, K. & Hille, B. Cannabinoids inhibit N-type calcium channels in neuroblastoma-glioma cells. *Proc. Natl Acad. Sci. USA* **89**, 3825–3829 (1992).
- Herkenham, M. *et al.* Cannabinoid receptor localization in brain. *Proc. Natl Acad. Sci. USA* **87**, 1932–1936 (1990).
- Devane, W. A. *et al.* Isolation and structure of a brain constituent that binds to the cannabinoid receptor. *Science* **258**, 1946–1949 (1992).
- Stella, N., Schweitzer, P. & Piomelli, D. A second endogenous cannabinoid that modulates long-term potentiation. *Nature* **388**, 773–778 (1997).
- Di Marzo, V. *et al.* Formation and inactivation of endogenous cannabinoid anandamide in central neurons. *Nature* **372**, 686–691 (1994).
- Di Marzo, V., Melck, D., Bisogno, T. & De Petrocellis, L. Endocannabinoids: endogenous cannabinoid receptor ligands with neuromodulatory action. *Trends Neurosci.* **21**, 521–528 (1998).
- Tsou, K., Mackie, K., Sañudo-Peña, M. C. & Walker, J. M. Cannabinoid CB1 receptors are localized primarily on cholecystokinin-containing GABAergic interneurons in the rat hippocampal formation. *Neuroscience* **93**, 969–975 (1999).
- Katona, I. *et al.* Presynaptically located CB1 cannabinoid receptors regulate GABA release from axon terminals of specific hippocampal interneurons. *J. Neurosci.* **19**, 4544–4558 (1999).
- Hajos, N. *et al.* Cannabinoids inhibit hippocampal GABAergic transmission and network oscillations. *Eur. J. Neurosci.* **12**, 3239–3249 (2000).
- Hoffman, A. F. & Lupica, C. R. Mechanisms of cannabinoid inhibition of GABA(A) synaptic transmission in the hippocampus. *J. Neurosci.* **20**, 2470–2479 (2000).
- Pitler, T. A. & Alger, B. E. Postsynaptic spike firing reduces synaptic GABA responses in hippocampal pyramidal cells. *J. Neurosci.* **12**, 4122–4132 (1992).
- Lenz, R. A., Wagner, J. J. & Alger, B. E. N- and L-type calcium channel involvement in depolarization-induced suppression of inhibition in rat hippocampal CA1 cells. *J. Physiol.* **512**, 61–73 (1998).
- Alger, B. E. *et al.* Retrograde signalling in depolarization-induced suppression of inhibition in rat hippocampal CA1 cells. *J. Physiol.* **496**, 197–209 (1996).
- Morishita, W. & Alger, B. E. Sr2+ supports depolarization-induced suppression of inhibition and provides new evidence for a presynaptic expression mechanism in rat hippocampal slices. *J. Physiol.* **505**, 307–317 (1997).
- Pitler, T. A. & Alger, B. E. Depolarization-induced suppression of GABAergic inhibition in rat hippocampal pyramidal cells: G protein involvement in a presynaptic mechanism. *Neuron* **13**, 1447–1455 (1994).
- Beltramo, M. *et al.* Functional role of high-affinity anandamide transport, as revealed by selective inhibition. *Science* **277**, 1094–1097 (1997).
- Piomelli, D. *et al.* Structural determinants for recognition and translocation by the anandamide transporter. *Proc. Natl Acad. Sci. USA* **96**, 5802–5807 (1999).
- Binz, T. *et al.* Proteolysis of SNAP-25 by types E and A botulinum neurotoxins. *J. Biol. Chem.* **269**, 1617–1620 (1994).
- Leung, S. M., Chen, D., DasGupta, B. R., Whiteheart, S. W. & Apodaca, G. SNAP-23 requirement for transferrin recycling in Streptolysin-O-permeabilized Madin-Darby canine kidney cells. *J. Biol. Chem.* **273**, 17732–17741 (1998).
- Weber, T. *et al.* SNAREpins: minimal machinery for membrane fusion. *Cell* **92**, 759–772 (1998).
- Lledo, P. M., Zhang, X., Südhof, T. C., Malenka, R. C. & Nicoll, R. A. Postsynaptic membrane fusion and long-term potentiation. *Science* **279**, 399–403 (1998).
- Lüscher, C. *et al.* Role of AMPA receptor cycling in synaptic transmission and plasticity. *Neuron* **24**, 649–658 (1999).
- Morishita, W., Kirov, S. A. & Alger, B. E. Evidence for metabotropic glutamate receptor activation in the induction of depolarization-induced suppression of inhibition in hippocampal CA1. *J. Neurosci.* **18**, 4870–4882 (1998).
- Morishita, W. & Alger, B. E. Differential effects of the group II mGluR agonist, DCG-IV, on depolarization-induced suppression of inhibition in hippocampal CA1 and CA3 neurons. *Hippocampus* **10**, 261–268 (2000).
- Vincent, P. & Marty, A. Neighboring cerebellar Purkinje cells communicate via retrograde inhibition of common presynaptic interneurons. *Neuron* **11**, 885–893 (1993).
- Cash, S., Zucker, R. S. & Poo, M. M. Spread of synaptic depression mediated by presynaptic cytoplasmic signaling. *Science* **272**, 998–1001 (1996).
- Wigström, H. & Gustafsson, B. Facilitation of hippocampal long-lasting potentiation by GABA antagonists. *Acta Physiol. Scand.* **125**, 159–172 (1985).
- Brody, D. L. & Yue, D. T. Relief of G-protein inhibition of calcium channels and short-term synaptic facilitation in cultured hippocampal neurons. *J. Neurosci.* **20**, 889–898 (2000).

Acknowledgements

We thank J. S. Isaacson and E. Schnell for suggesting a role for cannabinoids in DSI; R. S. Zucker for technical advice in the calcium uncaging experiments; and R. H. Scheller and Y. A. Chen for the gift of recombinant BTE light chain and SNAP-25. We are grateful for the comments on the manuscript contributed by D. S. Bredt, D. R. Copenhagen, R. H. Edwards, M. Frerking, D. Schmitz and M. P. Stryker. R.I.W. is supported by a National Science Foundation Graduate Research Fellowship. R.A.N. is a member of the Keck Center for Integrative Neuroscience and the Silvio Conte Center for Neuroscience Research. R.A.N. was supported by grants from the National Institutes of Health and the Bristol-Myers Squibb Corporation.

Correspondence and requests for materials should be addressed to R.A.N. (e-mail: nicoll@phy.ucsf.edu).

Ca²⁺ signalling between single L-type Ca²⁺ channels and ryanodine receptors in heart cells

Shi-Qiang Wang*, Long-Sheng Song*, Edward G. Lakatta* & Heping Cheng*†

* Laboratory of Cardiovascular Sciences, National Institute on Aging, National Institutes of Health, Baltimore, Maryland 21224, USA

† National Laboratory of Biomembrane and Membrane Biotechnology, College of Life Sciences, Peking University, Beijing 100871, China

Ca²⁺-induced Ca²⁺ release is a general mechanism that most cells use to amplify Ca²⁺ signals^{1–5}. In heart cells, this mechanism is operated between voltage-gated L-type Ca²⁺ channels (LCCs) in the plasma membrane and Ca²⁺ release channels, commonly known as ryanodine receptors, in the sarcoplasmic reticulum^{3–5}. The Ca²⁺ influx through LCCs traverses a cleft of roughly 12 nm formed by the cell surface and the sarcoplasmic reticulum membrane, and activates adjacent ryanodine receptors to release Ca²⁺ in the form of Ca²⁺ sparks⁶. Here we determine the kinetics, fidelity and stoichiometry of coupling between LCCs and ryanodine receptors. We show that the local Ca²⁺ signal produced by a single opening of an LCC, named a ‘Ca²⁺ sparklet’, can trigger about 4–6 ryanodine receptors to generate a Ca²⁺ spark. The coupling between LCCs and ryanodine receptors is stochastic, as judged by the exponential distribution of the coupling latency. The fraction of sparklets that successfully triggers a spark is less than unity and declines in a use-dependent manner. This optical analysis of single-channel communication affords a powerful means for elucidating Ca²⁺-signalling mechanisms at the molecular level.

To visualize the trigger Ca²⁺ entry through single LCCs in intact rat ventricular myocytes, we used confocal imaging in the line-scan mode to detect the local Ca²⁺ signal directly beneath the voltage-clamped patch membrane⁷ (Fig. 1, inset). The sarcoplasmic reticulum (SR) Ca²⁺ release was paralysed by 10 mM caffeine and 10 μM thapsigargin, an SR Ca²⁺ pump blocker. When the pipette solution contained 20 mM Ca²⁺ and 10 μM FPL64176 (FPL), an LCC agonist that prolongs channel open time^{8,9}, patch depolarization from a holding potential of –50 mV to test potentials between –40 and 0 mV activated single-channel currents (*i*_{Ca}) in a voltage-dependent manner (Figs 1 and 2a). Each open event was accompanied by a discrete minuscule Ca²⁺ transient, which we named a ‘Ca²⁺ sparklet’, in close proximity to the patch membrane. Ca²⁺ sparklets were resistant to ryanodine (10 μM, 5 min, *n* = 3 patches), but were completely abolished by the LCC antagonist, nifedipine (2 μM, 3 min, *n* = 3 patches). These data indicate that Ca²⁺ sparklets originate from single LCC openings, and represent the first optical measurement of voltage-gated single-channel activity in intact cells.

Unlike Ca²⁺ sparks of ryanodine receptor (RyR) origin, which typically last for ~30 ms (ref. 6), Ca²⁺ sparklets have a variable duration: the onset and termination of Ca²⁺ sparklets correlated tightly with the open and closure of the channel, respectively (Fig. 1). To characterize sparklet properties in relation to Ca²⁺ influx, we measured the ‘signal mass’ of sparklets (that is, the space-time integral of local Δ*F*/*F*₀ of a sparklet in the line-scan image), and integrated the corresponding unitary Ca²⁺ influx (*q*_{Ca}). Over the voltage range from –30 mV to +10 mV, at which LCC openings can be clearly identified, there was a linear correlation between *q*_{Ca} (~8,000–100,000 Ca²⁺ ions) and sparklet signal mass (Fig. 2b). Hence, Ca²⁺ sparklets provide a faithful readout of LCC unitary current.

In heart cells, Ca²⁺ sparklets from single LCCs are expected to deliver trigger signal into the 12-nm junctional cleft^{10,11} to activate